

Numerical simulation of a high viscosity bubble column

Danilo Carvajal^a, Victor Melendez-Vejar^a, Maik Irrázabal^a and Carlos Carlesi-Jara^a

^a Pontificia Universidad Católica de Valparaíso, Escuela de Ingeniería Química, Av. Brasil 2950,
Valparaíso 2340025, Chile
Email: danilo.carvajal@ucv.cl.

Abstract: The objective of this work is to develop fluid dynamic model to simulate a high viscosity bubble column for CO₂ absorption in Ionic Liquids (ILs). A very promising solvent for CO₂ capture and conversion are ionic liquids (ILs); ILs consist of a wide group of salts, which are liquids at room temperature, have low vapor pressure, high ionic conductivity and thermal stability. However, the use of ILs for industrial CO₂ depletion has a series of technical and economic issues that must be solved if this strategy is to be implemented. A very important drawback of ILs used for gas removal is its high viscosity, reaching values above 0.010 Pa·s which results in a decrease of the overall mass transfer rate and an increase in the power required for pumping and mixing. In order to elucidate the hydrodynamic behavior in a bubble column for CO₂ absorption with one gas feed inlet, a Computational Fluid Dynamic (CFD) model was developed, which was experimentally validated through a laboratory scale bubble column. To simplify the calculations and increase the accuracy of the results, the system was modeled as a single rising bubble which permits the estimation of the bubble rising velocity and the change of the bubble shape and size during its displacement. The model approach consists in a simplified two-dimensional multiphase flow model which considers the liquid solvent as a Newtonian fluid. The laminar, isothermal, and non-stationary hypotheses for both phases is applied. To model the displacement of the gas-liquid interface, the Level Set method was used. The laboratory tests were carried out using water-glycerol mixtures (58 %, 78 %, 84 % and 88 % by weight) and two Imidazolium type ionic liquids (pure [bmim]BF₄ and [bmim]PF₆). To compare the results obtained from the laboratory and the simulations, the drag coefficient for gas bubbles in liquids was used which correlates the fluid physical properties of fluids and the bubble equivalent diameter and terminal velocity. The results were also compared with predicted values obtained through a new correlation for the drag coefficient of single rising bubbles in ILs proposed by Dong et al. (2010). The results indicated that the CFD model is in good agreement with the experimental results, particularly for bubble Reynolds numbers below 5. Above this value, the model tends to underestimate the bubble terminal velocity which can be explained by the effect of the high velocity gradients close to the gas-liquid interface. Future steps will involve improving of the computational mesh, a parametric analysis of the reinitialization parameter and the parameter controlling the thickness at the interface transition zone. Acknowledgments. This work was supported by FONDECYT post-doc N°3120138 from CONICYT (Chile).

Keywords: *Computational Fluid Dynamic, Bubble Column, Ionic Liquid.*

1. INTRODUCTION

The continuous increase in CO₂ atmospheric concentration has caused a great concern in the scientific community because of its environmental hazard and its social implications. The European Union has set a target of 20% reduction of CO₂ emission by the year 2020; to meet this goal, a significant reduction in the CO₂ releases from fossil fuel will be required during the next years. This can be achieved by adopting an effective strategy for carbon capture, such as the use of liquids solvents for CO₂ capture. The ionic liquids present several characteristics which make them very interesting for CO₂ capture applications. However, when a gas is absorbed into an ionic liquid, typically the viscosity suffers an increase which has several negative impacts including the reduction of the species transport rate across the solvent and the increase the energy required for pumping and mixing. The physical properties of ILs may be modified by changing the substitute group in the cations and anions (Galán Sánchez *et al.*, 2007). During the gas absorption process, the increasing viscosity process may be controlled by a continuous removal of the solvent before the viscosity increases in a decontrolled way. There are very few theoretical and experimental investigations focusing on bubble columns using ILs as solvent one being the work by Dong *et al.* (2010), who conducted experiments using the ionic liquids [bmim]BF₄, [omim]BF₄ and [bmim]PF₆ at different operating conditions (i.e. temperature, gas flow rate and gas inlet diameter) in a bubble column fed with pure nitrogen. From the experimental results, they proposed a new correlation for the estimation of the drag coefficient as a function of Reynolds number and bubble aspect ratio as a function of a new dimensionless parameter; both correlations are particularly applicable to gas bubble formation in ionic liquids and demonstrated to be in good agreement with experimental results. Dong *et al.* (2010) then developed a coupled Computational Fluid Dynamic and Population Balance Model to study the mass transfer during CO₂ absorption in ILs (Wang *et al.*, 2010). However, there has been not undertaking as yet into investigation of bubble columns with ILs focused at the micro-scale level. An in-depth knowledge of the interface shape and displacement is important particularly of the mass transfer at a local scale.

2. EXPERIMENTAL SECTION

2.1. Test fluids and physical properties

Four water-glycerol mixtures (58 %, 78 %, 84 % and 88 % by weight) were prepared by stirring distilled water with the appropriate mass of glycerol for 60 min. Ionic liquids [bmim]BF₄ and [bmim]PF₆ were purchased from Iolitec GmbH (Denzlingen, Germany) with a purity of above 98 %. All the fluids were analyzed to determine density, viscosity and surface tension. All the measurements were carried out at 20°C to match the conditions of laboratory bubble column procedures. The density was measured using a pycnometer, the viscosity was obtained with an Ostwald viscometer (and compared with a rotational Fungilab viscometer) and the surface tension was measured with a stalagmometer. The physical properties of the tested fluids are listed in Table 1.

Table 1. Physical properties of the test fluids

Fluid	Description	Density, kg/m ³	Viscosity, Pa.s	Surface tension, N/m
A1	Glycerol 58 %	1155.2	0.0097000	0.0545711
A2	Glycerol 78 %	1211.8	0.0485300	0.0484380
A3	Glycerol 84 %	1224.5	0.1112900	0.0477220
A4	Glycerol 88 %	1282.2	0.2358300	0.0475000
A5	BmimBF ₄	1039.3	0.1117900	0.0289316
A6	BmimPF ₆	1276.4	0.3366855	0.0331631

2.2. Experimental setup

A schematic diagram of the experimental setup is depicted in Figure 1. The bubble column was made of transparent acrylic (Fig. 2) with a square base of 5 cm each side and 12 cm height (total volume of 300 ml). The column was tightly sealed to prevent leakage of both liquid and gas phases, and to avoid contamination with ambient air. The column has a thermal jacket (fluid: water) to maintain the temperature fixed at 20 °C. Pure nitrogen gas is injected through a single orifice in the bottom of the column. The gas flow rate is controlled by a mass flow controller, and, the gas flow rate constantly checked with a soap film meter. To produce different sizes of bubbles for each fluid tested; two diameters of orifice (0.8 mm and 1.25 mm) and two gas flow rates (7 ml/min and 20 ml/min) were applied. The size and shape of the bubbles were recorded with a digital camcorder (Panasonic HC V500M) set with a resolution of 1080 x 1920 pixels, 59.94 frames

per second (progressive) and 1/2000 s of shooter speed. To properly illuminate the column and avoid heating the column during the tests; a 30 W led lamp (equivalent to a 200 W halogen lamp) was used. To obtain good image quality (brightness and contrast) a semitransparent (white) acrylic panel was placed between the column and the video camera, which acted as a light diffusion filter. The image analysis was carried out through a MATLAB script developed by our workgroup. The script determine of the position and shape of the bubble in each frame of the recorded video file.

2.3. Testing procedure

Before starting the testing procedure, the column is washed and dried to eliminate all residues from previous tests, and then the testing fluid is injected inside the column from the top side until reaching a liquid level of 60 mm above the gas inlet orifice. The liquid is slowly injected to avoid the formation of bubbles which may hinder the recording process. By controlling the gas flow rate and stabilizing the frequency of formation of bubbles, the bubble motion is then recorded during 30s to obtain a wide sample of bubbles to analyse. Before and after each test, measurements of temperature and gas flow rate are performed.

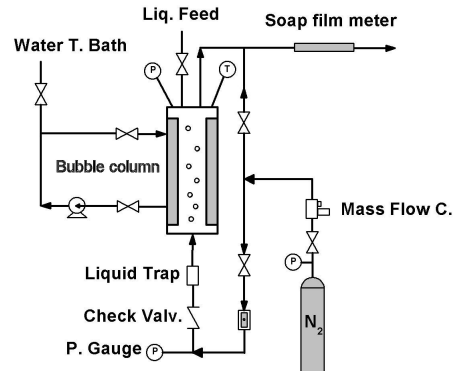


Figure 1. Flow diagram of the experimental set up.

3. CFD MODEL

3.1. Basic equations

The general assumptions for the model used are the laminar, incompressible and isothermal flows. The governing continuity and momentum equations for the two-phase flow are as follows:

$$\nabla \cdot \mathbf{u} = 0, \quad (1)$$

$$\rho \frac{\partial \mathbf{u}}{\partial t} + \mathbf{u} \cdot \nabla \mathbf{u} = -\frac{1}{\rho} \nabla p + \frac{\mu}{\rho} \nabla^2 \mathbf{u} + \mathbf{F}_v, \quad (2)$$

respectively, where ρ is the fluid density (kg/m^3), μ the dynamic viscosity ($\text{Pa}\cdot\text{s}$), \mathbf{u} is the velocity vector (m/s), t is time (s) and p the total pressure (Pa). The source term \mathbf{F}_v ($\text{kg/m}^2\text{s}$), includes the volumetric forces, such as the gravity force applied to the fluid over the whole domain and the surface tension to the gas-liquid interface.

3.2. Interface tracking model

To model the displacement of the gas-liquid interface, the Level Set method was used, which was introduced by Osher and Sethian (1988), for incompressible two phase flow. The motion of the interface is characterized through the scalar function ϕ , which is a smoothing function where $\phi = 0.5$ defines the position of the interface (COMSOL, 2012). For our model, $\phi = 0$ defines the gas phase, meanwhile $\phi = 1$ defines the liquid phase. The advection equation which defines the transport and reinitialization of ϕ through the entire domain is defined as follows:

$$\frac{\partial \phi}{\partial t} + \mathbf{u} \cdot \nabla \phi = \gamma \nabla \cdot \left(\epsilon \nabla \phi - \phi(1-\phi) \frac{\nabla \phi}{|\nabla \phi|} \right), \quad (3)$$

where the velocity vector (\mathbf{u}) is obtained from the numerical solution of the Navier-Stokes equations (equations 1 and 2). The reinitialization parameter γ determines the thickness of the interface transition zone

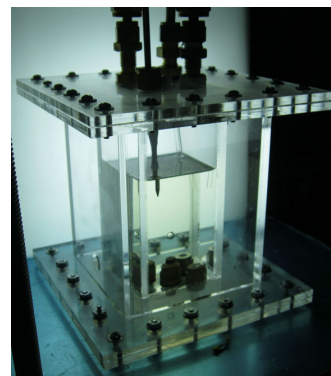


Figure 2. Photography of the laboratory scale bubble column.

where $0 < \phi < 1$. When stabilization techniques for the level set equation are used, it is recommended using a value of $\varepsilon = \mathbf{h}/2$, where \mathbf{h} is the typical size (m) of the mesh elements in the vicinity of the interface (Osher and Sethian, 1988). The γ parameter can be initially approximated by the maximum velocity magnitude of the system. The physical properties such as viscosity and density are estimated from a heaviside function which uses the properties of pure phases:

$$\rho = \rho_l + (\rho_g - \rho_l) \cdot \phi, \quad (4)$$

for the density and similarly for the viscosity:

$$\mu = \mu_l + (\mu_g - \mu_l) \cdot \phi, \quad (5)$$

where ρ_g , ρ_l , μ_g and μ_l are the density of the gas and the liquid, and viscosities of the gas and the liquid respectively. For the level set method, the surface tension and the gravity force are incorporated into the Navier-Stokes equations as volume forces in the source term of the momentum conservation equation (Eq. 2), which are defined as follows:

$$\mathbf{F}_v = \rho \cdot \mathbf{g} + \nabla \left[\sigma \left(\mathbf{I} + (-\mathbf{n} \cdot \mathbf{n}^T) \right) \delta \right], \quad (6)$$

where the first term on the right side defines the gravity force and the second the surface tension, σ is the surface tension (N/m), \mathbf{I} is the identity matrix and \mathbf{n} is a unitary normal vector to the interface with direction from the disperse phase to the continuous phase and is defined as follows (Deshpande, 2006):

$$\mathbf{n} = \frac{\nabla \phi}{|\nabla \phi|} \quad (7)$$

The level set parameter ϕ , is used to approximate the delta function δ through the following expression:

$$\delta = 6 \cdot |\phi(1-\phi)| \cdot |\nabla \phi| \quad (8)$$

3.3. Drag coefficient

In order to validate the results obtained from the CFD predictions, the drag coefficient obtained from the data produced during the laboratory tests are used. To compare de results with the literature, the drag coefficient correlation proposed by Dong et al. (2010) for bubbly flow using ionic liquids was used. The correlation was developed from experimental data using [bmim]BF₄, [omim]BF₄ and [bmim]PF₆ at different temperatures (37-82 °C, gas flow rate (0.1 – 5 ml/min) and gas inlet diameter (0.17, 0.47, 0.8 and 1.4 mm). The empirical expression for the drag coefficient (C_d) is based on two dimensionless numbers (i.e. Reynolds and Morton) and is defined as follows (Dong et al., 2010):

$$C_d = \mathbf{a} \cdot \mathbf{Re}^{\mathbf{b}} \cdot \mathbf{Mo}^{\mathbf{c}}, \quad (9)$$

where \mathbf{a} , \mathbf{b} and \mathbf{c} are defined as following:

For $0.5 \leq \mathbf{Re} \leq 5$: $\mathbf{a} = 22.73$, $\mathbf{b} = -0.849$, $\mathbf{c} = 0.020$, and for $5 < \mathbf{Re} \leq 50$: $\mathbf{a} = 20.08$, $\mathbf{b} = -0.636$, $\mathbf{c} = 0.046$. The use of these values will be termed Cd H.Dong (Table 2).

The drag coefficient for spherical bubbles is defined as following:

$$C_d = \frac{4 \cdot \mathbf{d}_e \cdot (\rho_l - \rho_g) \cdot \mathbf{g}}{3 \cdot \rho_l \cdot \mathbf{v}_t^2}, \quad (10)$$

where \mathbf{d}_e is the bubble equivalent diameter (m), and \mathbf{v}_t is the terminal rising velocity of bubble (m/s). Terminal velocity is reached when there is a balance between buoyancy and drag forces. The Reynolds number defined for a single rising bubble and Morton number are defined as:

$$\mathbf{Re} = \frac{\rho_l \cdot \mathbf{v}_t \cdot \mathbf{d}_e}{\mu_l}, \quad (11)$$

$$\mathbf{Mo} = \frac{\mathbf{g} \cdot \mu_l^4 \cdot (\rho_l - \rho_g)}{\sigma^3 \cdot \rho_l^2}, \quad (12)$$

respectively, where d_e is calculated as follows:

$$d_e = \sqrt[3]{d_x^2 \cdot d_y} \quad (13)$$

where d_x and d_y are the horizontal and vertical diameters (m) of the bubble, respectively.

3.4. Geometry and boundary conditions

The numerical domain has a height of 60 mm and a width of 40 mm. The size and aspect ratio of the initial condition of the interface gas-liquid is fixed according to the video recording from the experimental procedure (the first frame after the bubble detachment is used). The upper side of the fluid domain is defined as a zero pressure outlet. A non-slip condition is used for the walls. A representation of the geometry and boundary conditions are depicted in Figure 3.

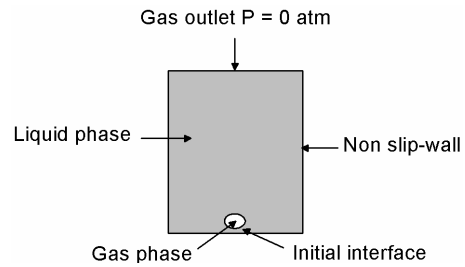


Figure 3. Geometry details and boundary conditions.

3.5. Numerical details

The CFD software COMSOL 4.2 was used for all the simulations. COMSOL uses the finite element method to discretize the partial differential equations defining the mathematical model. Both the geometry and the computational mesh were created in COMSOL. Different two-dimensional grids were tested and a final mesh of 17906 triangular cells was used. The mesh was refined to resolve regions of high gradients efficiently. The final minimum element size was approximately 0.09 mm in the interface displacement zone. The final element size ranges between 0.09 and 1.43 mm. A representation of the computational mesh is depicted in Figure 4.

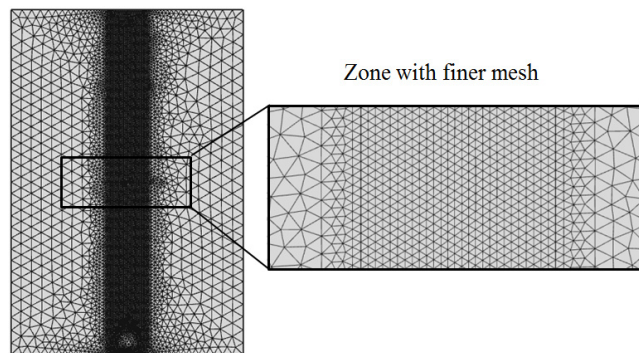


Figure 4. Computational mesh.

The system was defined as non-stationary and the total time needed for each simulation was 27.6 hours per second of simulation. The direct PARDISO solver was used for all simulations. Convergence was achieved when all normalized residuals of velocity and concentration reached values smaller than 10^{-3} . The simulations were performed on a HP Workstation with four 2.26 GHz Intel cores and 8 GB RAM. In order to ensure stability, the time step was fixed to 0.0001 s. The maximum number of iterations is reached when the relative tolerance exceeds 0.001 with respect of all variables.

4. RESULTS

4.1. Bubble rising velocity

After detachment, bubbles rise and suffering deceleration reaching a constant terminal velocity when a balance between buoyancy and drag forces is reached. From the experimental data and the simulations it is confirmed that a high viscosity

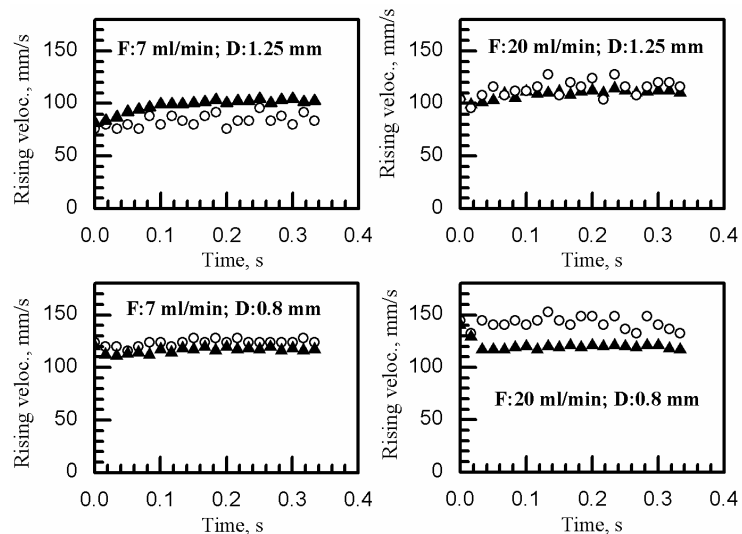


Figure 5. Bubble rising velocity evolution for 4 testing conditions using [bmm]BF₄ as liquid phase ($3.1 < Re < 8$). The triangles represent the CFD calculations and the circles the laboratory experiments.

leads to a decrease in rising velocity of bubbles. The CFD calculations for the bubble rising velocity presented good agreement with the experimental tests for several applied conditions, particularly for low Reynolds number, below 5. Most experimental fluids had viscosities above 0.1 Pa.s including the glycerol 84 % and 88 % w/w, the [bmim]BF₄ and [bmim]PF₆. Experimental and simulated bubble rising velocities for [bmim]BF₄ and [bmim]PF₆ samples are shown in Figure 5 and Figure 6 respectively. The figures show the high accuracy of the simulations for several conditions. However, when the Reynolds number exceeds a value of 5, the accuracy of the method decreases and the bubble terminal velocities are underestimated. The low accuracy of the CFD calculations at low viscosities can be explained from the effect of the high velocity gradients close to the interface gas-liquid. This problem was partially overcome by performing a finer computational mesh in the vicinity of the interface; however a further improvement of the model is necessary. Improvements would include a parametric analysis of the reinitialization parameter and the parameter controlling the thickness at the interface transition zone.

4.2. Model validation: Drag coefficient

The Drag coefficients and its associated Reynolds numbers calculated from the laboratory tests and the CFD simulations are graphically depicted in the Figure 7. As can be seen in the graph, experimental results clearly present a power law pattern between **Re** and **C_d**. Included in this relationship is the Morton number with which it is possible to estimate the coefficients of equation 9 using the least squares method giving the following parameters: for **Re** ≤ 5 : **a** = 58.66, **b** = -0.782, **c** = 0.185, and for **Re** > 5 : **a** = 4.601, **b** = -0.605, **c** = -0.1471. The use of these values in equation (9) will be termed **C_d fit** (Table 2). These parameters can be used to compare experimental results via eqn (9) with CFD simulations. The CFD

predictions are consistent with the experimental results for Reynolds numbers below 5. A high deviation between the experiments and CFD predictions were obtained for bubble Reynolds numbers above 20 (Figure 7). The comparison between the Drag coefficients calculated from the CFD model, experimental results using

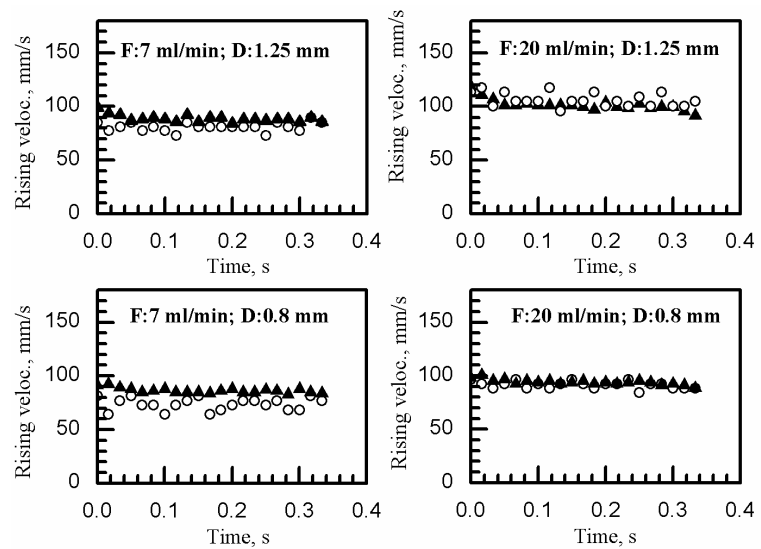


Figure 6. Bubble rising velocity evolution for 4 testing conditions using [bmim]PF₆ as liquid phase ($1.8 < Re < 3.0$). The triangles represent the CFD calculations and the circles the laboratory experiments.

Table 2. Drag coefficients for the tested ionic liquids with different conditions, using three different approaches: experimental, CFD and H.Dong correlation.

Fluid	V_t , mm/s	d_{eq} , mm	Re	Mo	C_d CFD	C_d fit experim	C_d H.Dong
bmim[BF ₄]	102.52	3.97	3.78	1.05E-03	4.93	5.83	6.41
bmim[BF ₄]	110.48	4.63	4.76	1.05E-03	4.96	4.87	5.27
bmim[BF ₄]	116.31	5.47	5.91	1.05E-03	5.28	4.31	4.73
bmim[BF ₄]	118.27	6.33	6.97	1.05E-03	5.92	3.90	4.26
bmim[PF ₆]	87.99	5.94	1.98	2.59E-03	10.02	11.41	11.30
bmim[PF ₆]	100.33	7.64	2.90	2.59E-03	9.91	8.46	8.16
bmim[PF ₆]	86.16	5.68	1.86	2.59E-03	10.00	12.00	11.93
bmim[PF ₆]	93.90	6.63	2.36	2.59E-03	9.83	9.94	9.73

the equation 9 and the Dong's correlation using equation is shown in Table 2. As can be seen in the table, at very low Reynolds number there is no a clear relationship between the deviation of the CFD results in respect to the experimental results. Given the limited amount of data available for this Reynolds number range, further testing is necessary, including lower gas flow rates and higher viscosity

5. DISCUSSION AND CONCLUSIONS

The CFD calculations for the bubble raising velocity presented good agreement in respect to the experimental tests for several applied conditions. In particular, this occurred for instances of Reynolds number below 5, most of experimental fluids had viscosities above 0.1 Pa.s, including, glycerol 84 % and 88 % w/w, the [bmim]BF₄ and [bmim]PF₆. When the Reynolds number exceeds a value of 5, the accuracy of the method decreases and the bubble terminal velocities are underestimated. The low accuracy of the CFD calculations at low viscosities can be explained from the effect of the high velocity gradients close to the gas-liquid interface which is related to deformation of the interface, which in turn affects the bubble rising velocity. Future experimentation and modeling will involve improvements in the computational mesh and a parametric analysis of the reinitialization parameter and the parameter controlling the thickness at the interface transition zone.

ACKNOWLEDGMENTS

This work was supported by FONDECYT N°1111000 project and FONDECYT post-doc N°3120138, both from CONICYT (Chile).

REFERENCES

- COMSOL (2012). Product information COMSOL Multiphysics 4.2, Stockholm.
- Deshpande, K. B., Zimmerman, W. B. (2006) "Simulation of interfacial mass transfer by droplet dynamics using the level set method. *Chemical Engineering Science* 61(19): 6486 – 6498.
- Dong, H., Wang, X., Liu, L., Zhang, X., Zhang S. (2010). The rise and deformation of a single bubble in ionic liquids. *Chemical Engineering Science* 65 (10): 3240 – 3248.
- Galán Sánchez, L. M., Meindersma, G. W. & de Haan A.B. (2007). Solvent properties of functionalized ionic liquids for CO₂ absorption, *Chemical Engineering Research and Design*, 85 (1): 31-39.
- Osher, S., Sethian J.(1988). Fronts propagating with curvature-dependent speed: Algorithms based on Hamilton-Jacobi formulations, *Journal of Computational Physics*, 79: 12-49.
- Wang, X., Dong, H., Zhang, X., Xu, Y., Zhang, S. (2010). Numerical simulation of absorbing CO₂ with ionic liquids. *Chemical Engineering Technology*, 33(10): 1615-1624.

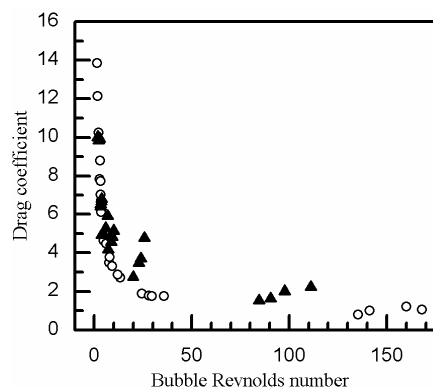


Figure 7. Drag coefficient vs. Reynolds number for several testing conditions (each point represent one test). The triangles represent the CFD calculations and the circles the laboratory experiments.